Journal of CO_2 Utilization 26 (2018) 552–563

Contents lists available at ScienceDirect

Journal of CO_2 Utilization

journal homepage: www.elsevier.com/locate/jcou

Solar thermochemical CO_2 splitting using cork-templated ceria ecoceramics

Fernando A. Costa Oliveira[a,*], Maria Alexandra Barreiros[a], Stéphane Abanades[b], Ana P.F. Caetano[c], Rui M. Novais[c], Robert C. Pullar[c]

[a] LNEG - Laboratório Nacional de Energia e Geologia I.P., LEN - Laboratório de Energia, Renewable Energy and Energy System Integration Unit, Estrada do Paço do Lumiar 22, 1649-038, Lisboa, Portugal

[b] Processes, Materials, and Solar Energy Laboratory (PROMES-CNRS), 7 Rue du Four Solaire, 66120, Font-Romeu, France

[c] Department of Materials and Ceramic Engineering/CICECO – Aveiro Institute of Materials, University of Aveiro, Campus Universitário de Santiago, 3810-193, Aveiro, Portugal

ARTICLE INFO

Keywords:
CO_2 splitting
Concentrated solar power
Ceria
Solar fuels
Thermochemical cycle
Cork

ABSTRACT

This work addresses the solar-driven thermochemical production of CO and O_2 from two-step CO_2-splitting cycles, using both ceria granules prepared from cork templates (CG) and ceria foams from polyurethane templates (CF). These materials were cycled in a high-temperature indirectly-irradiated solar tubular reactor using a temperature-swing process. Samples were typically reduced at 1400 °C using concentrated solar power as a heating source and subsequently oxidised with CO_2 between 1000–1200 °C. On average, CO production yields for CG were two times higher than for CF, indicating that the morphology of this three-dimensionally ordered macroporous (3-DOM) CeO_2 improves the reaction kinetics. Their performance stability was demonstrated by conducting 11 cycles under solar irradiation conditions. Slightly increasing the reduction temperature strongly enhanced the reduction extent, and thus the CO production yield (reaching about 0.2 mmol g^{-1} after reduction at 1450 °C in inert gas), while decreasing the oxidation temperature mainly improved the CO production rate (up to 1.43 µmol s^{-1} g^{-1} at 1000 °C). Characterisation of the 3-DOM structure, by means of XRD and SEM, provided insights into the reactivity behaviour of the developed materials. The pre-sintered ceria granules retained their structure after cycling. The fact that the mean cell size of CG is smaller (at least one order of magnitude) than that of CF suggests that its exposed surfaces enhanced reaction rates by a factor of two. Moreover, the maximum fuel production rate of CG was roughly three times greater than that reported previously for a ceria reticulated porous foam with dual-scale porosity.

1. Introduction

The conversion of sunlight directly to chemical fuels such as synthesis gas (or syngas – primarily a CO/H_2 mixture), hydrogen alone, or further to liquid fuels, offers the potential to efficiently store solar energy, transport it and utilise it on demand [1–3]. Thus, the generation of renewable solar fuels, derived from the sun, water and carbon dioxide and based on existing concentrated solar power (CSP) technology, is gaining considerable attention. The impact of solar fuels would be of utmost importance to ensure a sustainable energy future. Several methods for producing solar fuels, such as electrochemical, thermochemical and photochemical processes have been developed [4]. The use of solar radiation to drive a two-step thermochemical cycle based on redox materials benefits from the favourable thermodynamics arising from high temperature operation, the entire solar spectrum utilisation, the avoidance of the costly solar-to-electric conversion (used in electrolytic processes), and the elimination of CO/O_2 or H_2/O_2 gas separation. The latter is regarded as a tricky problem for one-step splitting methods [5]. Comprehensive literature reviews on solar thermochemical processes have been carried out [6–11]. Basically, two distinct types of metal oxides are being considered for the splitting of H_2O and/or CO_2: the volatile oxide cycles (ZnO/Zn or SnO_2/SnO) and the non-volatile oxide cycles such as Fe_3O_4/FeO or $CeO_2/CeO_{2-\delta}$. This study is focused on the cerium oxide redox pair.

On paper, the two-step cyclic process appears reasonably simple: concentrated solar radiation (a focused beam of sunlight) heats the metal oxide up to 1400 °C or more, driving its endothermic reduction and releasing oxygen. The reduced oxide is then cooled to 1000 °C or below (temperature-swing cycle), while a flow of steam and/or carbon dioxide re-oxidizes it, liberating hydrogen or carbon monoxide. Making such technology practical and cost-effective, however, poses noteworthy engineering challenges.

One of the most critical aspects is solar-to-fuel energy conversion efficiency, which in turn depends upon the redox material and the solar

* Corresponding author.
E-mail address: fernando.oliveira@lneg.pt (F.A. Costa Oliveira).

https://doi.org/10.1016/j.jcou.2018.06.015
Received 11 May 2018; Received in revised form 12 June 2018; Accepted 18 June 2018

thermochemical reactor design [12–14].

Among the several redox material candidates, there is as yet no clear winner because of the stringent performance requirements [15–21], namely favourable thermodynamics, fast kinetics and microstructural stability [22]. In recent years, several researchers have looked at ceria (CeO_2) redox materials, since they display high oxygen ion mobility and fast fuel production kinetics compared to ferrite-based and other non-volatile metal oxides [23,24]. The two step CO_2 or H_2O splitting cycle based on oxygen-deficient ceria encompasses (1) the solar thermal reduction (endothermal) that proceeds via the formation of oxygen vacancies and the release of gaseous O_2, resulting in the subsequent change in ceria stoichiometry (δ in $CeO_{2-\delta}$), and (2) the oxidation (ideally non-solar) that proceeds with CO_2 and/or H_2O when decreasing the operating temperature, thereby releasing CO and/or H_2 and re-incorporating oxygen into the lattice. The non-stoichiometry δ determines the fuel production yield and it is a function of temperature and oxygen partial pressure. Ceria can accommodate relatively large oxygen non-stoichiometries due to high capabilities in oxygen storage and mobility while the crystallographic fluorite structure remains stable [25]. As with most of the nonstoichiometric oxides, its thermochemical properties are directly influenced by the type and concentration of point defects [26]. To find the best performing materials, novel compositions are being developed combining constituents with morphologies promoting reaction efficiency. For instance, the limited reduction capacity of ceria can be improved through doping with other metals, such as Zr, in order to increase oxygen mobility by creating oxygen vacancies [27–31]. On the other hand, both the efficiency and the cycling rates in the solar reactor were found to be limited by thermal losses associated with the poor conductive and radiative heat transfer across the ceria structures [32,33]. Several morphologies with μm-size (such as macroporous materials, 3-DOM and felts) and mm-size (such as honeycomb monoliths and foams) porous structures have been examined [34–37]. However, if these structures are coated with metal oxides, they can undergo side reactions with the support, spallation and deactivation [38].

Another approach is to use naturally occurring and sustainable materials, such as wood (or wood wastes) and cork, as a template to create biomimetic/biomorphic ceramics, known as environmentally conscious ceramics, i.e. ecoceramics [39,40]. Of particular interest is the innovative work by Pullar et al. in creating cork-templated biomorphic ecoceramics of ferrites and ceria [41–43]. Cork is especially interesting as it has a very porous 3-DOM (three-dimensionally ordered macroporous) microstructure, consisting of elongated hexagonal cells ~20 μm diameter and 40–50 μm long [44]. The walls of these cells are only around 1 μm in thickness, resulting in an extremely porous, lightweight and regular microstructure, with up to 200 million cells per cm^3 [45].

Cork is the bark of a Mediterranean evergreen oak tree (*Quercus suber* L.), and Portugal supplies around 50% of the world's cork [46]. The cork layer is regenerated after each extraction from the tree every 9–13 years, and absorbs the equivalent amount of CO_2 which may be released from the cork during processing, with cork forests sequestering up to 5.7 T CO_2/ha/yr [44].

Eastern white pine was used as a template to produce ceria ecoceramics by Malonzo et al. [40]. The pine wood has elongated rectangular pores around 20 μm diameter with 10 μm wide cell walls, but when converted to an ecoceramic a large amount of the wood template was lost, resulting in a fragile material with cells of 20 μm diameter but with cell walls only 1 μm thick. Upon oxidation with CO_2 at 800 °C, this pine wood-templated CeO_2 reduced at 1400 °C then achieved CO production rates about 4 times higher than nonporous CeO_2 [40]. However, the cells were found to collapse with thermal cycling as grain growth caused the cell walls to fuse together, thereby reducing the active surface area. Furthermore, when the reduction temperature was raised to 1500 °C, CO production rates decreased by a factor of 7 compared to oxidation after reduction at 1400 °C (from 9 to 1.3 mL min^{-1} g^{-1}). Cork naturally has similar dimensions to the ecoceramic created by Malonzo et al. [40] (20 μm cells with 1 μm walls), yet with a more regular 3-DOM structure, and hence would appear to be an ideal template material. To our knowledge, there are no data available on the performance of ceria-based ecoceramics developed from cork substrates. In addition, the performance evaluation of reactive ceria structures in solar reactors under real and temporally-variable solar irradiation conditions has not been addressed so far.

In the present study, we report on the synthesis and experimental assessment of a novel form of biomimetic material – an ecoceramic produced from a cork template with the unique, highly porous cellular microstructure of cork – made of pure CeO_2 for CO production in an indirectly irradiated tubular solar reactor via concentrated solar heating. For comparison purposes, ceria foams manufactured by the replication method were also evaluated.

2. Experimental

2.1. Preparation of materials

Two ceria-based materials synthesised at both the University of Aveiro and LNEG were investigated in the form of granules and foams.

For this purpose, cork-template based-ceria granules (hereafter denoted as CG) were synthesised following a procedure described elsewhere [42], in which cork granules (typically of a size of several millimetres) were heat treated in a nitrogen atmosphere at 900 °C for 30 min to form carbon templates. These were then infiltrated with cerium nitrate solution ($Ce(NO_3)_3{\cdot}6H_2O$, 99%, Sigma Aldrich), dried overnight, and heated in air to 1600 °C for 30 min to remove the carbon, leaving a pure ceria ceramic while preserving the 3-DOM structure of cork.

Polymeric template ceria foams (hereafter called CF), of cylindrical shape (20 mm in diameter and 20 mm height), were manufactured by the replication method reported in detail elsewhere [47]. Briefly, an aqueous slurry with a solid content of 40 vol.% was prepared from cerium oxide powders (E. Merck, ref. 12446, Darmstadt, Germany, with an average particle size (d_{50}) of 1 μm, 99.9% purity and Fluka Chemica, ref. 22390, Buchs, Switzerland, d_{50} = 0.2 μm, purity > 99%; 50 wt% of each) together with 0.8 wt% dispersant (Targon 1128, BK, Ladenburg, F.R. Germany). Additions of 1 wt. % sodium bentonite (MO34, Chemicer, Spain) and 1 wt. % kaolinite (supplied by Rauschert Portuguesa Ltd.) powders were made for structure stabilisation to prevent the collapse of the foam structure during polymer removal. They were mixed together for 12 h in an alumina ball mill jar (solids/ball ratio of 1:4). The resulting stock slurry was then used to impregnate an open-cell polyurethane (PU) foam (grade 20DB, manufactured by Flexipol – Espumas Sintéticas S.A., Portugal). The mean cell size of PU foam was determined to be ~700 μm (36 ppi) by using image analysis and its density is 21 kg m^{-3} [48]. After drying under controlled temperature and humidity conditions overnight, the samples were heated at 1 °C min^{-1} to 500 °C for 1 h and subsequently sintered at 1450 °C for 30 min. The same foams were also prepared without any structure stabiliser additives for comparison purposes (hereafter referred to as CFBL; i.e. binder less).

2.2. Thermochemical activity testing

The activity of the synthesised materials was first investigated by thermogravimetric analysis performed in controlled atmospheres (TG, Setaram Setsys Evo 1750). About 150 mg of sample was placed in a platinum crucible hung inside the furnace chamber (the foam was preliminary crushed into small parts before being loaded in the crucible). The TG chamber was then evacuated to eliminate residual air and filled with argon gas flowing at 20 mL min^{-1} (99.999% purity). The reduction step was carried out at 1400 °C (heating rate of 20 °C min^{-1}), held for 45 min, and the mass change was registered

continuously. Then, the temperature was lowered to 1050 °C in Ar, and held for 60 min, for the re-oxidation step at isothermal conditions. For this purpose, the CO_2 stream was injected from the auxiliary gas inlet and mixed with argon, the carrier gas, at a total flow rate of 20 mL min^{-1}. The mixture (50% CO_2 in Ar) entered at the top of the furnace chamber towards the sample and then exited the chamber at the bottom. CO_2 gas reacted with the oxygen-deficient material to produce CO. The same cycle was repeated twice and this procedure was then applied for each tested material. The reduction temperature was chosen because it will be the nominal operation temperature of the tested solar reactor. Although a higher reduction yield could be obtained at a higher temperature, the main issues would be linked to the reactant losses by sublimation and to constraints of thermal stability for the materials of the solar reactor and the reactive material itself.

The mass losses during thermal reduction are converted to the mole amount of O_2 released per gram of ceria according to:

$$nO_2 = \Delta m_{loss}/(MO_2 \cdot m_{ceria}) \quad (1)$$

where Δm_{loss}, is the mass variation measured by TG; MO_2, the molecular weight of O_2; and m_{ceria}, the mass of ceria used in each experiment.

The reduction yield (X_{red}) is calculated as follows:

$$X_{red} = nO_2/nO_{2;max} \quad (2)$$

with

$$nO_{2;max} = 1/(4M_{ceria}) \quad (3)$$

where $nO_{2,max}$ is the maximum amount of O_2 (mol g^{-1}) that could be released if Ce^{4+} was completely reduced to Ce^{3+} (i.e. $\delta_{max} = 0.5$), and M_{ceria} is the molecular weight of ceria. Hence, X_{red} quantifies the fraction of Ce atoms in the oxidation state Ce^{3+} ($X_{red} = \delta/\delta_{max}$ with $\delta_{max} = 0.5$).

The mass gain associated with CO_2 splitting results in a CO amount (mol g^{-1}) which can be calculated as:

$$nCO = \Delta m_{gain}/(M_O \cdot m_{ceria}) \quad (4)$$

with Δm_{gain}, the mass gain during the re-oxidation step, and M_O, the atomic weight of oxygen.

The oxidation yield (α) is calculated based on the mass variation of the re-oxidation step and the reduction yield, as follows [49]:

$$\alpha = \frac{2\,nCO\ M_{ceria}}{X_{red}} \quad (5)$$

2.3. Solar thermochemical CO_2-splitting cycles

The experimental setup used was developed for investigating high-temperature solid–gas thermochemical reactions in controlled atmospheres using a solar chemical reactor mounted on a medium size solar furnace (MSSF) facility at CNRS-PROMES. It is described in detail elsewhere [50,51] and it is shown in Fig. 1. Briefly, concentrated solar energy was used to drive the thermochemical redox reactions involving ceria, especially the endothermal reduction step (the oxidation step can practically be performed during cooling without any solar energy supply). The high-temperature process heat was supplied by a horizontal axis solar furnace consisting of a sun-tracking heliostat reflecting the incident solar irradiation towards a 2 m diameter parabolic dish concentrator. The solar reactor consisted of a cavity receiver with 15 mm diameter aperture positioned at the focal point of the concentrator for the optimal access and absorption of concentrated solar radiation. The maximum incident thermal power absorbed by the cavity through the aperture is about 1.5 kW for a DNI of 1 kW m^{-2} (only a fraction of this energy was necessary to reach the maximum operating temperature). The cavity made of graphite was lined with a surrounding insulation layer and shielded from the surrounding

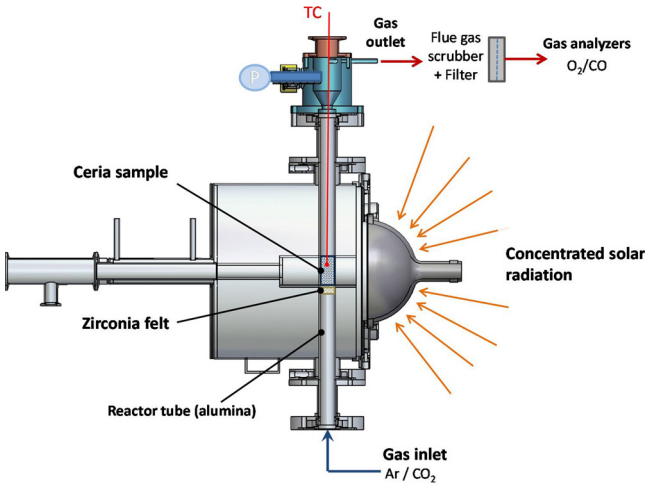

Fig. 1. Schematic and photograph of the solar reactor for the two-step solar-driven thermochemical cycles.

atmosphere using a transparent Pyrex glass window. The samples (either cork-templated ceria granules or ceria foam, about 8 g) were analysed inside a 20 mm diameter alumina tube crossing vertically the cavity. They were supported using a 3 mm thick ZrO_2 felt disc (Zircar Inc., USA) that is chemically inert under the operating conditions to avoid unwanted side reactions. The reaction temperature measurements were carried out using an alumina-shielded B-type thermocouple positioned directly within the reacting sample inside the alumina tube. This corresponds to the reaction temperature because the cavity-type solar reactor configuration provides homogeneous temperature distribution in the reacting zone where the sample is placed (40 mm in height). Additional temperature measurements were performed by B-type thermocouples (at the cavity external walls and through the reactor insulation) and by a solar-blind pyrometer (pointing to the tube external wall) to confirm temperature homogeneity. Purge gas (Ar, 99.999% purity, O_2 content below 2 ppm) and CO_2 (99.995% purity) flowrates were regulated using electronic mass flow controllers. Reduction flow rate was set at 0.25 N L min^{-1} of argon whereas the oxidation step was performed at 0.1 N L min^{-1} CO_2 and 0.1 N L min^{-1} Ar (i.e. 50% CO_2 in Ar), to keep the residence time of reacting gas constant during each cycle. These gases were fed from the bottom of the tube and the product gases exited from the reactor at the top.

Prior to each test, residual air in the reactor chamber was eliminated by successive vacuum pumping and refilling with Ar in order to operate in inert atmosphere inside the tube thereby improving the reduction yield by decreasing the oxygen partial pressure. The reactor was first heated in Ar up to the targeted reduction temperature (~1400 °C). The reduction (endothermic) step consisted of heating the material up to 1400 °C, with a set heating rate (~30–40 °C/min), and maintaining a

temperature plateau for ~15 min until the outlet O_2 concentration became low enough (below 100 ppm), meaning that the reduction was complete and the equilibrium state in the material oxygen stoichiometry was reached. The temperature was controlled by adjusting the opening of a shutter placed between the heliostat and the concentrator, thereby tuning the solar energy input to achieve the targeted temperature. The O_2 evolution was measured continually using an oxygen analyser with zirconium oxide sensor (SETNAG™ JC48 V, scale: 10–10000 ppm, precision: 0.2%, calibrated with 5040 ppm O_2 in N_2). Then, the temperature was lowered by readily closing the shutter for the re-oxidation (exothermic) step, and CO_2 (balanced with Ar) was injected into the reactor chamber to react with the oxygen-deficient material and to produce CO. The soaking time of the oxidation step at T = 1000 °C was also set at roughly 15 min to reach reaction completion. CO concentration in the exhaust gas was measured on-line (concentration as a function of time profiles) by a specific analyser with NDIR sensor (MGA3000, full scale: 0–30% for CO, repeatability ± 1% full scale). The amounts of gas produced were then determined by time integration of the gas production rates. Each material was subjected to a minimum of 6 cycles (6 for CF and 11 for CG).

2.4. Characterisation of materials

X-ray diffraction (XRD) analyses were performed, prior to and after thermochemical testing using a Panalytical XPert Pro MPD diffractometer in Bragg-Brentano configuration. The data were collected with a step size of 0.02° using a X'Celerator 1D detector with CuKα radiation. Samples were observed by scanning electron microscopy (SEM) using a Philips XL30 FEG (field emission gun), before and after thermochemical cycles, in order to check for morphology changes. SEM secondary electron images were obtained at an acceleration voltage of 5–10 kV. For this study, the samples were not coated with any conductive surface layer. Semi-quantitative elemental composition was obtained with an EDS (EDAX) system equipped with a Si(Li) detector and a 3 µm super ultra-thin window (SUTW). Spectra were collected at an acceleration voltage of 30 kV for 300 s acquisition time.

3. Results and discussion

3.1. Reactivity performance

The reducibility and CO_2-splitting ability of the CeO_2 samples were assessed via successive cycles in a thermobalance at atmospheric pressure. The data of a typical TG run of a CG sample is shown in Fig. 2.

During the heating process up to 1400 °C, the reduction begins at around 1030 °C corresponding to a sharp mass loss. The reaction rate markedly increases with increasing temperature. On approaching the set temperature, the Δm curve exhibits an inflection point, indicating a gradual reaction deceleration. This is attributed to the rate-limiting transition between reduction at the surface and in the bulk of ceria [52]. The peak rate of O_2 production was 0.06 µmol s^{-1} g^{-1} (measured at the maximum of the derivative of the mass variation). The reduction is a thermally activated process that proceeds with continuous oxygen disincorporation from the oxide lattice as the temperature is increased. The reduction rate thus immediately decreases when the temperature rise is stopped. At the end of the isothermal plateau at 1400 °C, the reduction was not complete as the mass loss was still progressing after 45 min of temperature dwell (the reduction duration was however not expanded to keep reasonable cycling durations). Upon cooling to 1050 °C in Ar, the reduction stopped and the mass remained stable. CO_2 was then injected at the plateau causing a sharp mass increase because of prompt oxygen incorporation in the oxide lattice, with a peak CO production rate of 0.59 µmol s^{-1} g^{-1} (thus about 10 times higher than the peak O_2 production rate). The oxidation reaction is thus significantly faster than reduction, which is in line with findings for other ceria materials [36,49]. The mass uptake amounts to 90% of maximal value after about 12 min. After 60 min injecting CO_2 at dwell temperature, the sample mass approximates a steady value matching almost full re-oxidation. Table 1 summarises the calculated reduction and oxidation yields (pure ceria powder was also included for comparison).

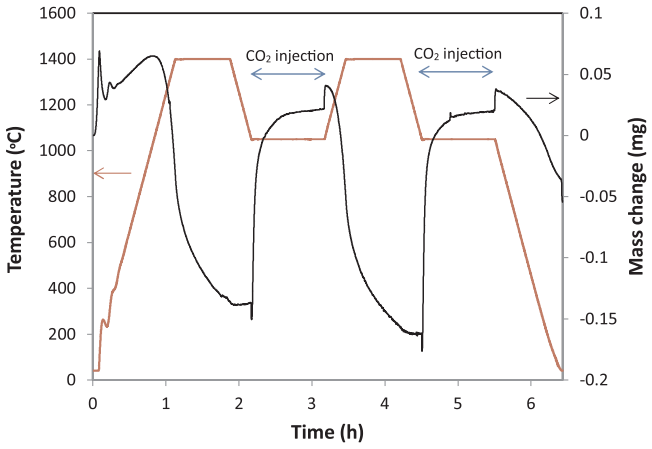

Fig. 2. Typical TG data of two consecutive thermochemical cycles obtained for CG showing the temperature profile, CO_2 injection periods and corresponding mass change vs. time.

During the reduction step at 1400 °C, the amount of oxygen released is 51 µmol g^{-1}, corresponding to a reduction yield of 3.5%, which is in good agreement with data reported previously [49]. A similar reactivity is observed for the crushed CF materials, since the reduction yield (2nd cycle) is equal to that obtained for both CG and pure ceria dispersed powder. The similar reactivity of the raw ceria materials is explained by their similar shaping as powdered samples to fit the small crucible volume (130 µl) of the TG system. However, a discrepancy is observed for CF samples depending whether or not additives were used in the synthesis method, which is particularly evident in the first reduction cycle (the mass loss is higher in the presence of additives that may thus form reduced compounds upon heating in inert gas). The presence of the small amount of inorganic additives (2 wt. %) required to prevent the collapse of the structure of the ceria foams upon burning out of the polymeric template slightly decreased the CO production capacity, when compared with a similar foam structure prepared without adding any binding additives. On the second reduction cycle, however, the reduction yield is equal to that obtained for pure ceria. This suggests that the additives should not have a significant effect on the reactivity of ceria during successive CO_2-splitting thermochemical cycles. On the other hand, the values of α are in line with those anticipated for pure ceria indicating that re-oxidation was almost complete regardless of the tested materials. The maximum mass loss for CG was around 0.22 mg based on the initial sample mass of 124.5 mg, which corresponds to a non-stoichiometric δ value of 0.03 (e.g. $CeO_2 \rightarrow CeO_{2-\delta}$), i.e. consistently lower than that obtained for CeO_2 powders reduced at 1450 °C for 8 h followed by oxidation at 1100 °C [53]. The goal was here to maintain reasonable and shorter cycling durations for practical implementation. It is thus not relevant to use extended durations, as this would not reflect realistic operating conditions used in real solar reactors. The cycling durations were thus chosen to be able to perform cycles in a reasonable time and were typically high enough to reach significant reaction extent. Since oxygen-deficient ceria is totally re-oxidised, the CO productivity cannot be improved unless increasing the reduction temperature for enhanced oxygen vacancies formation. Alternatively, decreasing the oxygen partial pressure (by vacuum pumping or sharp inert gas dilution) can also be used to increase the reduction yield (pressure swing cycle). In this study we did not choose to operate under such harsh conditions to give realistic insights into the capabilities of ceria for CO_2 splitting in a real solar reactor. Thus the nominal temperature was 1400 °C and atmospheric pressure operation

Table 1
Oxygen and CO production yields during two thermochemical cycles investigated with TGA for CG, CF (with and without binders) and comparison with a reference CeO_2 powder [49].

	O_2 released at 1400 °C				CO produced at 1050 °C			
	1 st cycle		2nd cycle		1 st cycle		2nd cycle	
	μmol O_2/g	X_{red} (%)	μmol O_2/g	X_{red} (%)	μmol CO/g	α (%)	μmol CO/g	α (%)
CFBL	51	3.5	51	3.5	81	79.4	95	93.1
CF	117	8.1	51	3.5	59	25.4	84	81.7
CG	51	3.5	51	3.5	86	84.7	98	96.7
CeO_2 powder	51	3.5	53	3.7	102	100.0	105	99.0

was selected for both cycle steps.

The reduction from Ce^{4+} to Ce^{3+} causes the crystal lattice to expand since Ce^{4+} (0.097 nm) exhibits a smaller ionic radius than Ce^{3+} (0.114 nm) [54]. The resulting stress suppresses further reduction [55].

The reduction or oxidation yield can be enhanced e.g., by doping or by increasing the material surface area, respectively [56]. Regardless of the material structure and morphology, the main limitation of the ceria redox cycle is the thermal reduction step as pure ceria can hardly be reduced at elevated δ (δ is generally limited to 0.02–0.05 unless using extremely high temperatures or low operating pressures) but it is readily oxidised. The reactivity of the structured materials was then studied in a solar reactor in order to unveil the effect of their different morphologies and macroscale shapes.

3.2. Solar thermochemical CO_2-splitting

The redox performances of ceria-based materials were investigated in the solar reactor under real solar irradiation conditions. Both the O_2 and CO rate evolutions as well as the measured temperatures (inside the reactant T_{tube} and at the cavity external wall T_{wall}) are shown in Fig. 3. The temperature of the reduction step was about 1400 °C and was controlled by adjusting the shutter opening in response to the dynamic variations of the DNI (due to the diurnal transient evolution or to instabilities resulting from clouds passage). However, a time delay occurred because of the thermal inertia of the reactor and the indirect heat transfer of solar radiation to the reactive material via the intermediate alumina tube wall. Thus the temperature change in the material as a result of the shutter opening variation was noticed only after about one minute, which explains why the precise dynamic control of the reaction temperature is a tricky task when using real solar-heated reactors. The oxidation temperature was different from one cycle to another and was shown to significantly affect the amount of CO produced. Typically, for thermodynamic limitation reasons, the temperature gap between reduction and oxidation must be high enough to favour the CO production step. The thermodynamic barrier can indeed be counteracted by enhancing the temperature swing to activate the re-oxidation step at the expense of kinetic limitations that may arise and additional sensible heat losses. Consequently, the oxidation temperature was varied in the range 1000–1200 °C. The operating pressure was constant throughout the cycles and was slightly above the atmospheric pressure to avoid any air contamination inside the system (0.85 bar at the experimental site elevation, pressure drop across the reactor of about 0.01 bar). The oxygen content in the system was thus always below 10 ppm (except when O_2 was released during the ceria reduction step).

The thermochemical redox cycling of the materials was performed via temperature swing by alternatively switching the gas atmosphere between Ar for reduction and CO_2 (50% in Ar) for oxidation. Regarding the ceria foam (8.65 g of CF) in Fig. 3a, the reduction was performed at a maximum temperature of 1400 °C and the average O_2 production was about 30-35 μmol g^{-1}, thus lower than the value measured in TG, which may be due to temperature inhomogeneity in the foam structure that greatly affects the reduction extent. This can be attributed to the large mass difference of material being processed between TG and solar experiments (about 60 times greater in the solar reactor), as well as the different material structure (crushed foam in TG), thereby affecting the heat and mass transfer, and the maximum reaction extent during reduction. The first cycle showed a limited CO production, in accordance with the TG results, which may be linked to the presence of binding additives that modifies the reactivity. However, the CO productivity increased in subsequent cycles and varied between 50–75 μmol g^{-1} depending mainly on the oxidation temperature and the extent of the previous reduction step. Typically, the maximum CO production rate increased when decreasing the oxidation temperature. For example, the peak rate of CO production was 2.1×10^{-3} NL min^{-1} (0.18 μmol s^{-1} g^{-1}) at 1200 °C (4th cycle) and 1.14×10^{-2} NL min^{-1} (0.98 μmol s^{-1} g^{-1}) at 1000 °C (last cycle). The O_2 production rate (~0.04 μmol s^{-1} g^{-1}) was much lower than the CO production rate as expected. The CO/O_2 molar ratio was sometimes higher than 2, which can be simply explained by the incomplete oxidation occurring in previous cycles (especially the first one), thereby providing additional oxygen vacancies available for the subsequent cycles. Thus the CO production was not directly correlated to the O_2 production in the previous reduction step, but rather to the total amount of oxygen lost and recovered from the first cycle.

Regarding the cork-templated ceria (8.33 g of CG), two consecutive series of thermochemical redox cycling were performed during different days without removing the material from the reactor (total of 11 cycles), shown in Fig. 3b–c. In the first series performed with a poor DNI (~750 W m^{-2}) and depicted in Fig. 3b, the maximum temperature was limited during the 1st cycle (1360 °C) and the last cycle (1320 °C). As a result, the reduction extent was much lower in these than the other cycles (2nd, 3rd and 4th cycles in Fig. 3b) performed at 1400 °C. The amount of CO produced was also directly related to the temperature of the reduction step (the higher the reduction temperature, the higher the produced CO). The amount of O_2 produced was consistent with the TG measurements (~51 μmol g^{-1} in the 4th cycle), and a slight temperature increase over 1400 °C directly improved the O_2 production (2nd and 3rd cycles in Fig. 3b). The oxidation temperature was varied and greatly influenced the CO production rate. Indeed, the peak of CO production was significantly broadened (a slower rate but over a longer period), but with a slightly smaller quantity produced, when increasing the oxidation temperature to 1200 °C (113.9 μmol g^{-1} for the 4th cycle at 1200 °C, compared to 138.0 μmol g^{-1} for the 3rd cycle at 1100 °C in Fig. 3b). These CO yields correspond to more than twice the CO yield from CF material under the same conditions. With a lower oxidation temperature of only 1000 °C in the last cycle in Fig. 3b, an even narrower peak resulted (with a production of only 68.9 μmol g^{-1} owing to the lower reduction temperature of 1320 °C). Therefore, the peak rate of CO production increased when decreasing the oxidation temperature below 1200 °C, while the oxidation duration was shortened (as evidenced by the sharpened CO production peak).

In the second cycling series performed at a high DNI (~1000 W m^{-2}) in Fig. 3c, the reduction temperature was increased up to 1450 °C

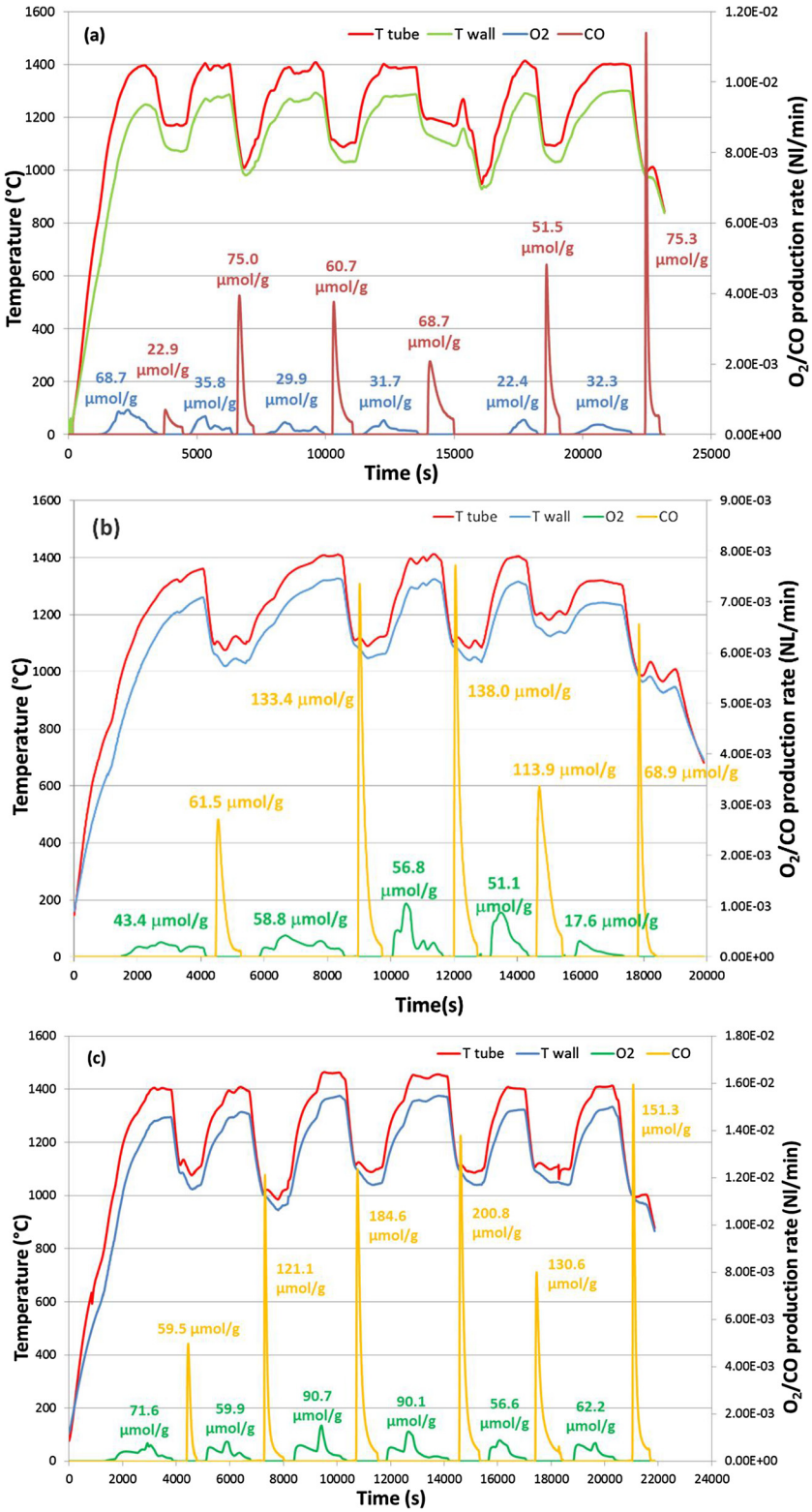

Fig. 3. Time-dependent solar thermochemical reduction and re-oxidation profiles for (a) ceria foam (6 cycles at DNI ~ 900 W m^{-2}), (b) ceria granules with cork structure (1st series of 5 cycles at DNI ~ 750 W m^{-2}), (c) ceria granules with cork structure (2nd series of 6 cycles at DNI ~ 1000 W m^{-2}).

(3rd and 4th cycles), which greatly impacted the reduction yield. O_2 production reached over 90 µmol g^{-1}, representing a 50% increase of the reduction extent when compared with that at 1400 °C (~60 µmol g^{-1} in the 2nd, 5th and 6th cycles), with a peak O_2 production rate of 0.13 µmol s^{-1} g^{-1} in the 3rd cycle, which in turn also increased the subsequent maximum CO production yield. The peak CO production rate was up to 1.6×10^{-2} NL min^{-1} (1.43 µmol s^{-1} g^{-1}) in the last cycle performed at an oxidation temperature of 1000 °C. Consequently, the cycling stability of the ceria-based materials was demonstrated under real solar irradiation conditions. The reduction temperature strongly influenced the reduction extent, and thus in turn, the CO production yield, while the oxidation temperature mainly affected the

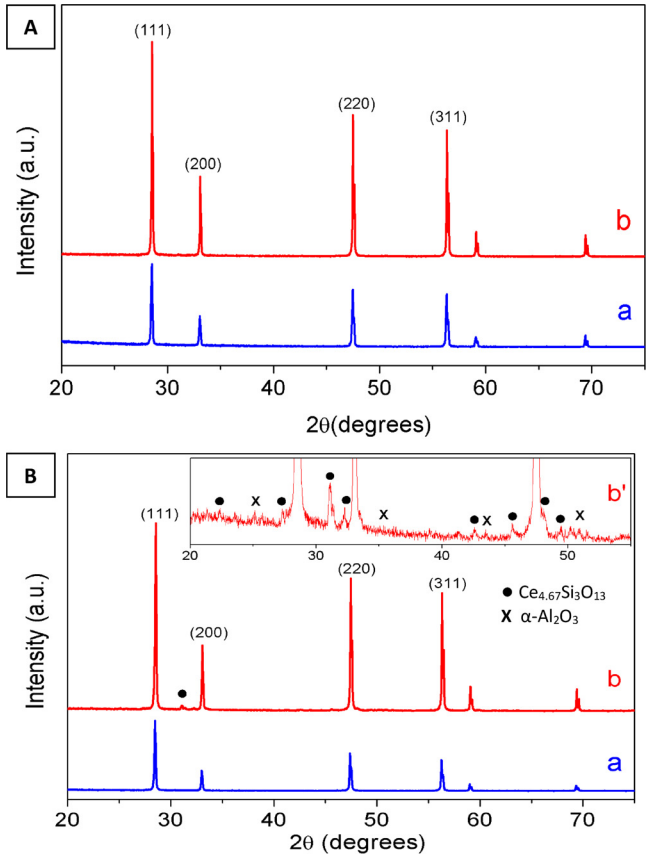

Fig. 4. XRD patterns for CG (A) and CF (B) before (a) and after (b) thermochemical cycles (inset b' shows small peaks not observed in curve b).

CO production rate.

The CG material produced a cumulative amount of O_2 and CO of 659 and 1364 μmol g^{-1} over 11 cycles, thus yielding a CO/O_2 ratio of about 2 (equal to the theoretical ratio). The enhanced redox activity and CO_2 splitting capacity of the cork-templated ceria material when compared with the porous ceria foam under the same conditions was revealed.

The amounts of CO produced during the CO_2-splitting step using CG were as high as ~200 μmol g^{-1} and the CO production stability was maintained during cycling, suggesting that the morphology of the ceria-based material does affect the redox performance. Indeed, porous structures are known to favour the oxidation step due to their high surface areas [36]. The observed reaction rate enhancement by a factor of around two from CF to CG might be attributed to the fact that the mean cell size of CG is much smaller (at least one order of magnitude) than that of CF. The reaction extent, in turn, is not only limited by the thermodynamics, in particular the temperature and oxygen partial pressure, but also by other factors such as thermal and mass transport. Transport properties are affected by fundamental material physical properties (such as thermal diffusivity and thermal conductivity) as well as material morphology (like size and shape of pores). Besides, the reaction rate was also directly correlated with temperature. Indeed, increasing the reduction temperature by merely 50 °C (from 1400 to 1450 °C) resulted in an increase of O_2 yield from 60 to 90 μmol g^{-1} as illustrated in the case of CG. Consequently, the amount of CO formed was in the range of 185–200 μmol g^{-1}; higher than that observed at 1400 °C (in the range of 120–150 μmol g^{-1}) corresponding to about a 35–55% increase, as expected. The oxidation kinetics was also made faster by decreasing the temperature to 1000 °C. This means the oxidation is favoured when decreasing the temperature (thus increasing the temperature gap between redox steps) in accordance with thermodynamic predictions. For example, the last cycle was performed at an oxidation temperature of 1000 °C for each material and showed the highest CO production rate. The oxidation reaction is significantly faster than the reduction, as seen in Fig. 3. The CO production rate exhibits a sharpened peak as soon as CO_2 is injected and then the CO production decreases steadily (the total peak duration is around 10–15 min). In contrast, the O_2 production rate is highly sensitive to small temperature variations and it features a broadened pattern, fluctuating in response to small temperature variations. The total duration of O_2 release (around 30 min) corresponds to both the heating up time to the maximum temperature, and the holding time at this temperature. The reduction releasing O_2 is immediately triggered when the CO_2 injection is stopped and the temperature is increased, but the O_2 release evolves smoothly.

For a ceria reticulated porous foam with dual-scale porosity [2], the peak O_2 evolution rate was 0.19 mL min^{-1} g^{-1} (0.14 μmol s^{-1} g^{-1}), and peak CO release rate was 0.75 mL min^{-1} g^{-1} (0.56 μmol s^{-1} g^{-1}) using a reduction step over 1500 °C. This fuel production rate was thus almost three times lower than the CO production rate obtained here with CG at a lower reduction temperature, while the total specific CO release was similar (around 200 μmol g^{-1}). These results point out the superior reactivity of the cork-structured ceria material CG studied here when compared with ceria porous foam with single-scale [38] or dual-scale porosity [2,36].

Specific yields of O_2 and CO convey important information for the reactor design [12]. Since the CO_2 splitting process requires minimum temperatures typically in excess of 1400 °C (at atmospheric pressure), the reactor vessels must resist under stringent operating conditions (high temperatures, oxidising and reducing conditions) for several thousands of cycles annually. This implies that the construction materials as well as the reactive materials must function with high efficiency while remaining thermally stable against temperature changes (resistance to high temperature and thermal stresses). Hence, the reduction temperature was kept as low as possible (< 1450 °C) in order to prevent grain growth leading to pore closure of the reactive material. Another option would be to operate under a combined temperature/pressure swing mode in order to reduce the operating temperature while maintaining the same fuel productivity by decreasing the total pressure during reduction (δ is increased as temperature is increased or pO_2 is decreased) [21]. This option further results in reduced heat losses (because the temperature swing is lowered) and reduced thermal constraints on the materials. Conversely, pressure swing (vacuum pumping) should be applied at each cycle since the oxidation step should better proceed at atmospheric pressure, which induces additional energy consumption and thus may hardly be a viable option for large-scale industrial implementation.

3.3. Microstructural characterisation

To aid in the interpretation of the reactive properties of both CF and CG, all samples were characterised after thermochemical cycling.

The XRD patterns confirm that both materials unambiguously present a cubic fluorite structure typical of pure ceria (Fig. 4). Best match of peaks was obtained for ICCD card no.034-0394. Additionally, in the case of CF after thermochemical cycles, minor peaks could be ascribed to $Ce_{4.67}Si_3O_{13}$ (ICDD card no.071-0829) and α-Al_2O_3 (ICDD card no. 46-1212). This is corroborated by observations made by means of SEM/EDS (as will be discussed below). Exposure to temperatures as high as 1450 °C caused CG samples to experience crystallite size growth, as evidenced by the sharpening of reflections in the XRD patterns (Fig. 4). Based on Scherrer equation applied to (111) diffraction peaks, mean crystallite sizes were estimated to be 56 and 60 nm for CF whereas an increase was observed for CG from 55 to 86 nm before and after thermochemical cycling, respectively.

The initial and final morphologies of CF and CG, paired with the observed performance above, yield significant insight into the

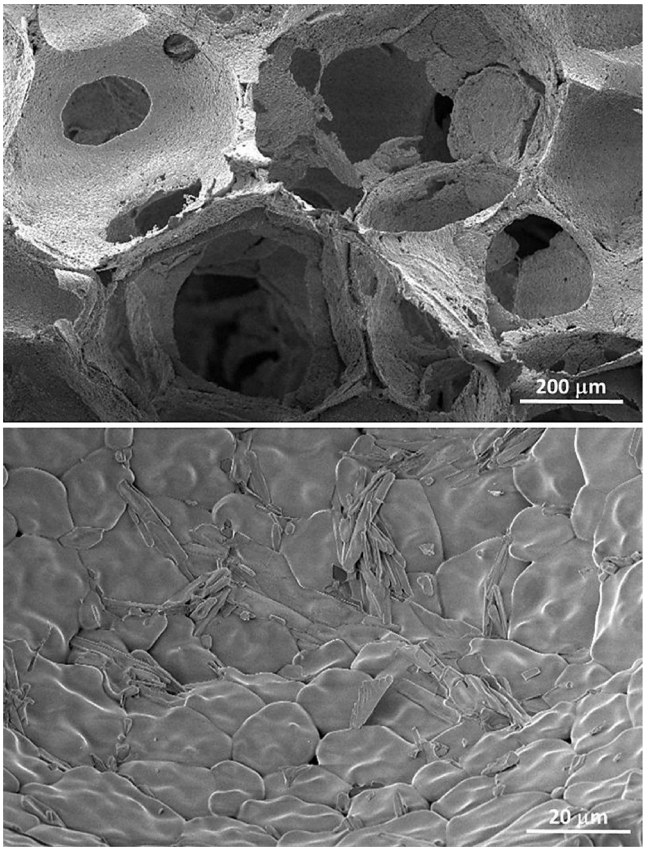

Fig. 5. SEM micrographs of CF after exposure to two consecutive thermochemical cycles on the TG apparatus (T_{red} = 1400 °C, 45 min; T_{oxi} = 1050 °C, 60 min).

behaviour of these materials under thermal cycling.

Evidence of needle-like crystals on the surface of the closed cell walls making the 3D porous structure of CF suggests that mullite might have formed resulting from the additives required to prevent the collapse of this structure (Fig. 5). Although not apparent, the bulk density of the CF material was determined to be 1.01 ± 0.13 g cm^{-3} (based on mass and volume measurements). This corresponds to a porosity of ~86%, taking into account that the ceria density measured by helium pycnometry was 7.15 g cm^{-3}. The formation of needle-like crystals was also observed in the case of iron-coated mullite foams used as burner substrates under radiant mode conditions [57]. This would account for the low CO yields obtained for CF during the first cycle, both in the thermobalance and at the MSSF facility. Upon reheating, however, the specific CO yields were similar to those obtained in successive thermal cycles suggesting that their effect on the overall performance of CF is negligible. Bearing in mind that in the reduction step the oxygen partial pressure is very low and the temperatures are as high as 1400 °C, it is likely that the needle-like crystals with a large aspect ratio may have grown at the surface of cell walls and struts via a vapour-liquid-solid mechanism. Indeed, in an inert atmosphere, a eutectic reaction in the system Al_2O_3-$Ce_2Si_2O_7$ was found to occur at 1375 °C [58]. Heating CeO_2 in an inert atmosphere would require temperatures in excess of 1700 °C to reduce it to Ce_2O_3 [59]. Therefore, the presence of impurities, such as Fe, Mg, Ca, and most importantly Na, are likely to play an important role in the liquid phase formation observed in CF samples. Hence, the formation of a transient liquid phase containing CeO_2, SiO_2, and Al_2O_3 should not be ruled out, in the case of the CF.

By comparison, CG after heating to 1600 °C had a measured density of only 0.41 ± 0.08 g cm^{-3} (~6% of theoretical density), which is equivalent to a high degree of porosity of ~94%, i.e. 8% higher than that of CF. In addition, the density of bulk ceramic disks of ceria, pressed from a commercial powder and sintered at 1600 °C, had a density of 6.66 ± 0.07 g cm^{-3} (~93% of theoretical density), around 16 times greater than that observed for CG.

No additives were used in preparing CG samples and, therefore, features related to this were not observed. Indeed, a cork-like

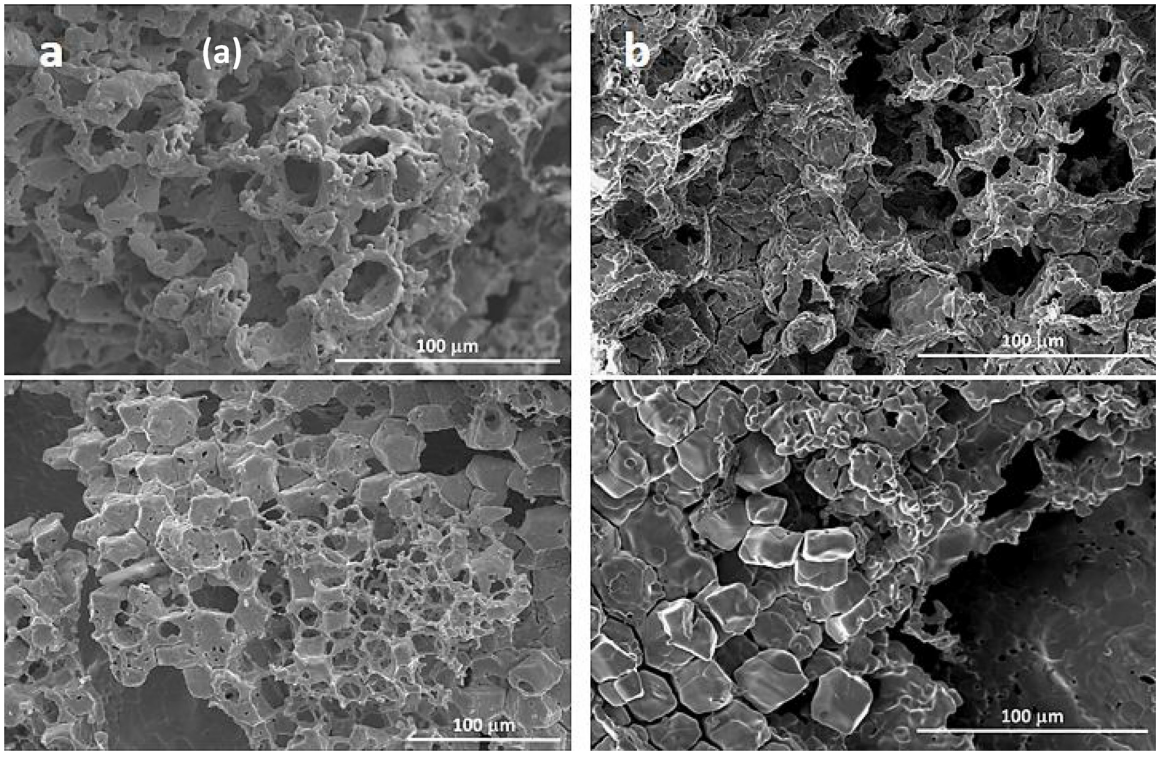

Fig. 6. Representative SEM micrographs of CG depicting the structural and morphological changes observed prior to (a) and after (b) thermochemical cycles.

microstructure was maintained in much of the CG material, with cells of ~25 μm diameter and relatively thin cell walls, despite the grain growth which occurred during their heat treatment at 1600 °C (Fig. 6), thus explaining that no significant loss in reactivity performance was observed in repetitive cycling. However, it was observed that in much of the material an "inverse" cork structure has formed, in which the ceria was in dense pieces with the form of the interior of the cells, separated by gaps equivalent to the original cell walls (Fig. 6a). This is a result of difficulties during the infiltration process in the synthesis of CG, as an excess of ceria precursor solution has flooded the carbonised cork skeleton, and filled some of the pores completely. It can be seen that both the porous cork structure, and this non-porous "inverse" cork structure, co-exists in the same granule of CG (Fig. 6b). Further optimisation of this material, and avoidance of this "inverse" cork structure, will inevitably result in further enhancement of their redox abilities for CO_2 splitting.

It is well established that, at high temperatures, CeO_2 is unstable; this primarily manifests itself as changes in its texture characteristics [60]. In particular, the specific surface area of CeO_2 usually decreases depending on preparation and calcination conditions [61,62]. The shift between the Ce^{3+} to Ce^{4+} states also results in the formation of lattice defects and high oxygen mobility in the ceria lattice, which in turn can lead to a strong catalytic potential.

No significant changes in morphology were observed for CF as shown in Fig. 7. The microstructure of the as-sintered CF shows the typical features of ceramic foams produced by the replication method, in particular the hollow nature of the struts which can be seen in Fig. 7a. Although the grain size remained small (< 5 μm), the residual porosity is low owing the fine powder used (d_{50} below 1 μm) making it very reactive at the sintering temperature of 1450 °C. After thermal cycling, grain growth has occurred through an Ostwald ripening mechanism. This is particularly evident in Fig. 7b, where it can be seen that Ostwald ripening produced a more uniform structure with larger grains growing at the expense of the smaller ones. Unlike what was observed after the TG cycles, no evidence of needle-like crystals was noticed on CF surface. Instead, a network of intergranular pockets

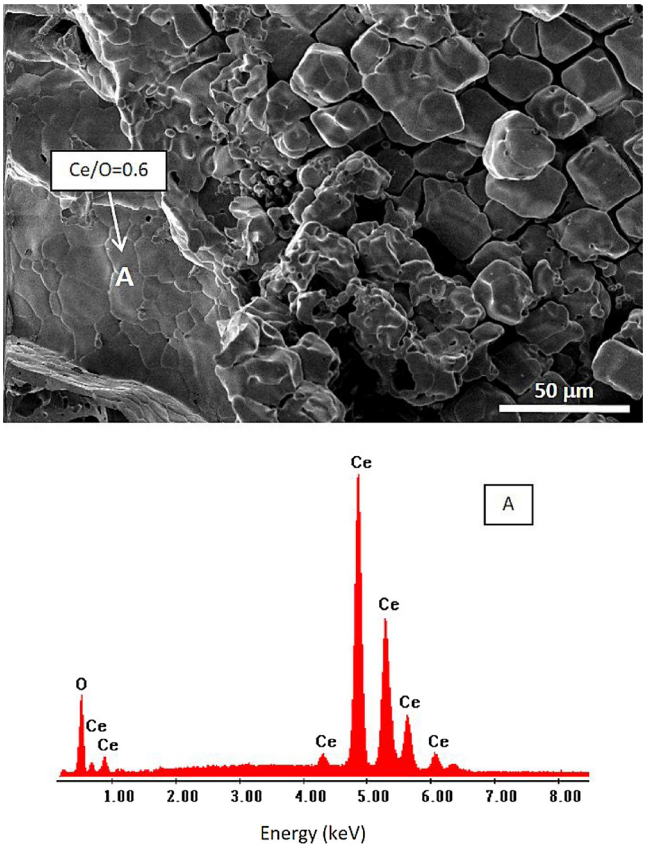

Fig. 8. Surface morphology SEM micrograph of CG after thermochemical cycles showing typical features including localised reduction of CeO_2 to $CeO_{2-\delta}$ corroborated by evidence gathered by semi-quantitative EDS spot analysis.

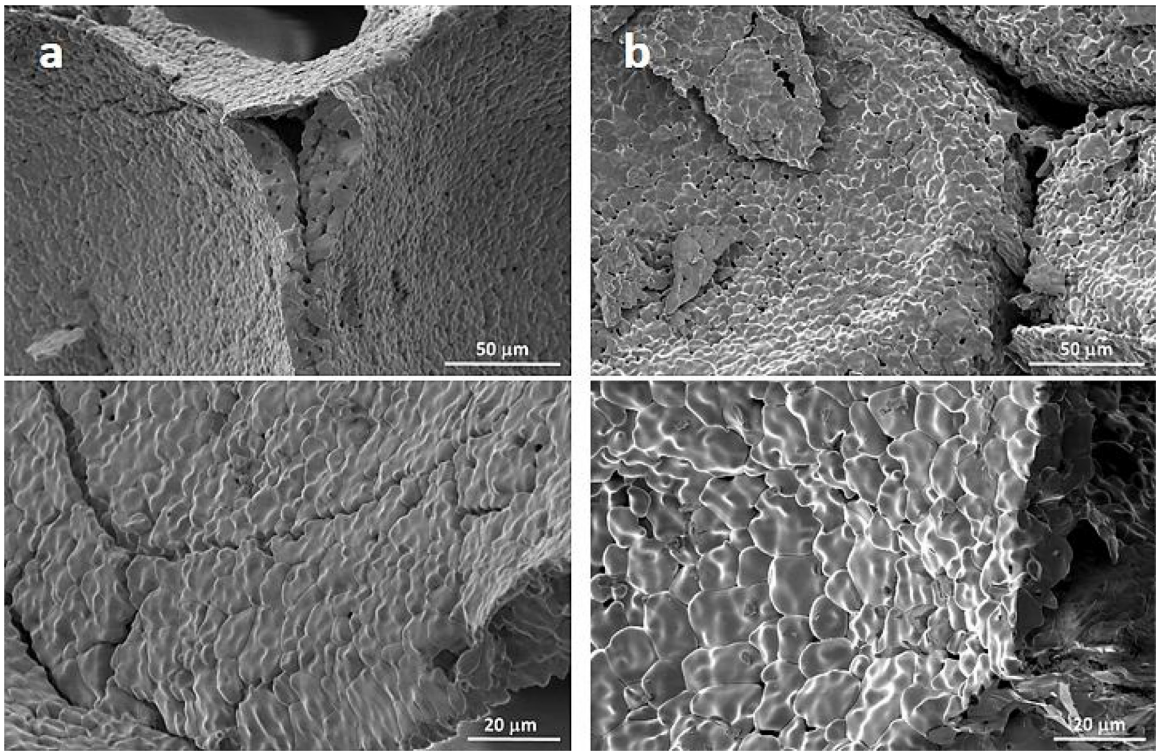

Fig. 7. Representative SEM micrographs of CF depicting the structural and morphological changes observed prior to (a) and after (b) thermochemical cycles.

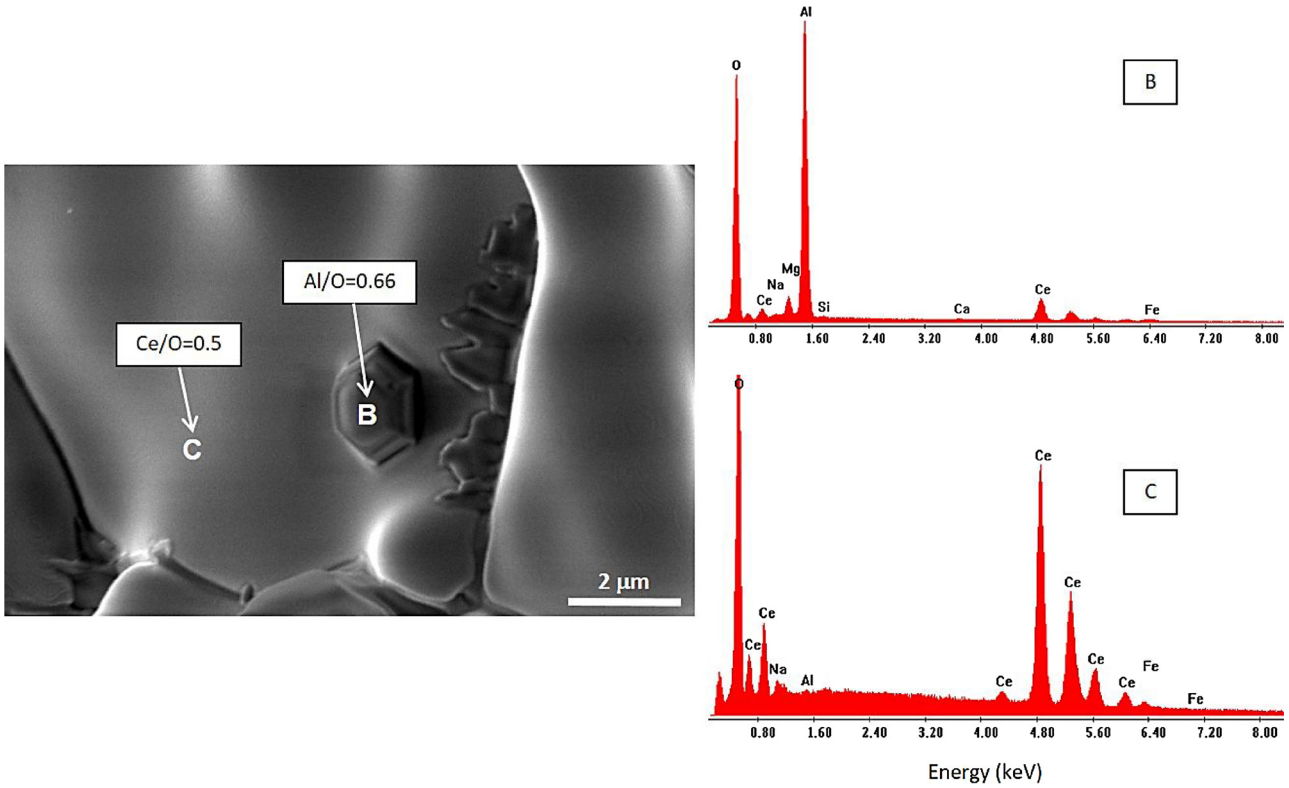

Fig. 9. Surface morphology SEM micrograph of CF after thermochemical cycles showing hexagonal Al_2O_3 crystal according to evidence gathered by semi-quantitative EDS spot analysis (atomic Ce/O and Al/O ratios are indicated).

(< 1 µm in size) formed, preferentially located at triple joints of grains, and consisting mainly of cerium silicate. This is related to outward diffusion of additive cations to the surface. However, such a change in surface texture was rather localised, and did not significantly influence the reaction rates.

Another interesting feature was noticed with CG after cycling. Semi-quantitative EDS revealed the presence of a phase containing an oxygen atomic content smaller than that expected for stoichiometric CeO_2, suggesting the presence of $CeO_{2-\delta}$ phase (Fig. 8).

On the other hand, EDS analysis on CF after cycling (Fig. 9) provided results consistent with the relative atomic Ce/O ratio for stoichiometric CeO_2 and allowed us to determine, on a hexagonal structure, an atomic ratio compatible with the presence of an Al_2O_3 crystal, due to the additives used.

The 3-DOM cork-templated ceria allowed increasing the CO production yields, but this is hindered both by the portion of initial CG ceria ecoceramic which did not possess the biomorphic cork structure, and the degree of densification resulting from the high temperature required for reducing CeO_2. Despite this, CG activity and cyclical stability were not altered, and the processing of these cork-derived ceria ecoceramics must be optimised to fully replicate the cork structure, and efforts made to minimise grain growth, for instance, through the doping of CeO_2. This requires the development of materials having high surface area based upon an interconnected pore network, which must be retained over many thousands of cycles and hours of operation at temperatures in excess of 1400 °C. Further advancements in material properties are indeed still of critical importance [21,63] coupled to the need for numerical modelling of thermal transport, thermochemical reactions, and thermomechanics in high-temperature solar thermochemical systems [64,65]. Another approach would be to envisage multistage thermal reduction in order to significantly increase the efficiency of solar-thermochemical production [66].

4. Conclusions

Two CeO_2 materials with differing morphologies were evaluated for CO_2 splitting under solar thermochemical cycling. After a reduction step at 1400 °C in inert gas, the CO yield of cork-templated ceria was found to be about twice that of its ceria foam counterpart. Although appreciable grain growth did occur upon thermal cycling, its effect on the reaction kinetics, fuel productivity and cyclical stability was shown to be negligible over the 11 cycles studied. It was shown that during reduction, oxygen release occurred at a much slower rate than that at which CO was evolved during the oxidation step. The CO production rate also increased when decreasing the oxidation temperature while the CO yield was not significantly affected. In contrast, the CO yield was directly linked to the reduction extent (i.e. the amount of oxygen non-stoichiometry), and thus to the reduction temperature. The superior CO_2-splitting activity and noticeable chemical stability of the cork-templated ceria was demonstrated by a global CO/O_2 ratio of 2 achieved after conducting 11 cycles. The differences in reactivity between the two materials investigated here were chiefly related to surface availability for the solid-gas reactions. It can also be inferred that surface rather than bulk diffusion of oxygen ions is the rate controlling mechanism. This is attributed to the lack of an interconnected porosity network responsible for a large solid-gas interface. Typically, the surface area of both materials is less than 1 $m^2\ g^{-1}$, which is unavoidable for such high-temperature applications in which materials sintering is commonly encountered. Since the cell size of the cork-templated ceria granules is about one order of magnitude smaller than that of their porous foam counterparts, and with the denser packing of the portion which had lost the cork microstructure, it can be inferred that these features contributed to the higher specific CO yields of the cork-templated sample compared to foam. In fact, the cork-derived ceria, in which the mean cell size is at least one order of magnitude smaller than that of the polymer-derived ceria, also had enhanced reaction rates that were two times larger. The improved reactivity and performance

stability of this novel class of ceria-based materials prepared from a cork template was demonstrated during repeated solar-driven CO_2-splitting cycles, which provides a suitable and reliable alternative material for the operation of high temperature solar chemical reactors.

Acknowledgements

The authors would like to acknowledge the EU through the seventh framework program for the financial support of this work under the STAGE-STE project with contract number 609837 and the SFERA II project (Grant Agreement number 312643). National funding provided by FCT, in the frame of the H2CORK project, grant no. PTDC/CTM-ENE/6762/2014 as well as POCI-01-0145-FEDER-016862 is also gratefully acknowledged. Thanks are also due to Amorim Cork Composites, S.A. and Flexipol – Espumas Sintéticas S.A. for donating the cork samples and the PU foams, respectively. One of us, RMN, is supported by a post-doc research fellowship in the frame of the H2CORK project. RCP wishes to thank FCT grant IF/00681/2015 for supporting this work. This work was developed within the scope of the project CICECO-Aveiro Institute of Materials, POCI-01-0145-FEDER-007679 (FCT Ref. UID/CTM /50011/2013), financed by national funds through the FCT/MEC and co-financed by the EU with FEDER funds under the PT2020 Partnership Agreement.

References

[1] C. Graves, S.D. Ebbesen, M. Mogensen, K.S. Lackner, Sustainable hydrocarbon fuels by recycling CO_2 and H_2O with renewable or nuclear energy, Renew. Sustain. Energy Rev. 15 (2011) 1–23, http://dx.doi.org/10.1016/j.rser.2010.07.014.

[2] D. Marxer, P. Furler, J. Scheffe, H. Geerlings, C. Falter, V. Batteiger, A. Sizmann, A. Steinfeld, Demonstration of the entire production chain to renewable kerosene via solar thermochemical splitting of H_2O and CO_2, Energy Fuels 29 (2015) 3241–3250, http://dx.doi.org/10.1021/acs.energyfuels.5b00351.

[3] P. Lanzafame, S. Abate, C. Ampelli, C. Genovese, R. Passalacqua, G. Centi, S. Perathoner, Beyond solar fuels: renewable energy-driven chemistry, Chem. Sus. Chem. 10 (2017) 4409–4419, http://dx.doi.org/10.1002/cssc.201701507.

[4] Z. Wang, R.R. Roberts, G.F. Naterer, K.S. Gabriel, Comparison of thermochemical, electrolytic, photoelectrolytic and photochemical solar-to-hydrogen production technologies, Int. J. Hydrog. Energy 37 (2012) 16287–16301, http://dx.doi.org/10.1016/j.ijhydene.2012.03.057.

[5] T. Nakamura, Hydrogen production from water utilizing solar heat at high temperatures, Sol. Energy 19 (1977) 467–475, http://dx.doi.org/10.1016/0038-092X(77)90102-5.

[6] E.A. Fletcher, Solarthermal processing: a review, J. Sol. Energy Eng. 123 (2001) 63–74, http://dx.doi.org/10.1115/1.1349552.

[7] A. Steinfeld, Solar thermochemical production of hydrogen – a review, Sol. Energy 78 (2005) 603–615, http://dx.doi.org/10.1016/j.solener.2003.12.012.

[8] L. Xiao, S.-Y. Wu, Y.-R. Li, Advances in solar hydrogen production via two-step water-splitting thermochemical cycles based on metal redox reactions, Renew. Energy 41 (2012) 1–12, http://dx.doi.org/10.1016/j.renene.2011.11.023.

[9] C. Agrafiotis, M. Roeb, C. Sattler, A review on solar thermal syngas production via redox pair-based water/carbon dioxide splitting thermochemical cycles, Renew. Sustain. Energy Rev. 42 (2015) 254–285, http://dx.doi.org/10.1016/j.rser.2014.09.039.

[10] D. Yadav, R. Banerjee, A review of solar thermochemical processes, Renew. Sustain. Energy Rev. 54 (2016) 497–532, http://dx.doi.org/10.1016/j.rser.2015.10.026.

[11] T. Kodama, S. Bellan, N. Gokon, H.S. Cho, Particle reactors for solar thermochemical processes, Sol. Energy 156 (2017) 113–132, http://dx.doi.org/10.1016/j.solener.2017.05.084.

[12] N.P. Siegel, J.E. Miller, I. Ermanoski, R.B. Diver, E.B. Stechel, Factors affecting the efficiency of solar driven metal oxide thermochemical cycles, Ind. Eng. Chem. Res. 52 (2013) 3276–3286, http://dx.doi.org/10.1021/ie400193q.

[13] M. Lange, M. Roeb, C. Sattler, R. Pitz-Paal, Efficiency assessment of a two-step thermochemical water-splitting process based on a dynamic process model, Int. J. Hydrog. Energy 40 (2015) 12108–12119, http://dx.doi.org/10.1016/j.ijhydene.2015.07.056.

[14] E. Koepf, I. Alxneit, C. Wieckert, A. Meier, A review of high temperature solar driven reactor technology: 25 years of experience in research and development at the Paul Scherrer institute, Appl. Energy 188 (2017) 620–651, http://dx.doi.org/10.1016/j.apenergy.2016.11.088.

[15] T. Kodama, N. Gokon, R. Yamamoto, Thermochemical two-step water splitting by ZrO_2-supported $Ni_xFe_{3-x}O_4$ for solar hydrogen production, Sol. Energy 82 (2008) 73–79, http://dx.doi.org/10.1016/j.solener.2007.03.005.

[16] M.D. Allendorf, J.E. Miller, A.H. McDaniel, Design of materials for solar-driven fuel production by metal-oxide thermochemical cycles, Electrochem. Soc. Interface 22 (2013) 63–68, http://dx.doi.org/10.1149/2.F06134if.

[17] J.R. Scheffe, R. Jacot, G.R. Patzke, A. Steinfeld, Synthesis, characterization, and thermochemical redox performance of Hf^{4+}, Zr^{4+}, and Sc^{3+} doped ceria for splitting CO_2, J. Phys. Chem. C 117 (2013) 24104–24114, http://dx.doi.org/10.1021/jp4050572.

[18] J.R. Scheffe, A. Steinfeld, Oxygen exchange materials for solar thermochemical splitting of H_2O and CO_2: a review, Mater. Today 17 (2014) 341–348, http://dx.doi.org/10.1016/j.mattod.2014.04.025.

[19] J.E. Miller, A. Ambrosini, E.N. Coker, M.D. Allendorf, A.H. McDaniel, Advancing oxide materials for thermochemical production of solar fuels, Energy Procedia 49 (2014) 2019–2026, http://dx.doi.org/10.1016/j.egypro.2014.03.214.

[20] C.N.R. Rao, S. Dey, Generation of H_2 and CO by solar thermochemical splitting of H_2O and CO_2 by employing metal oxides, J. Solid State Chem. 242 (2016) 107–115, http://dx.doi.org/10.1016/j.jssc.2015.12.018.

[21] R.J. Carrillo, J.R. Scheffe, Advances and trends in redox materials for solar thermochemical fuel production, Sol. Energy 156 (2017) 3–20, http://dx.doi.org/10.1016/j.solener.2017.05.032.

[22] W.C. Chueh, C. Falter, M. Abbott, D. Scipio, P. Furler, S.M. Haile, A. Steinfeld, High-flux solar-driven thermochemical dissociation of CO_2 and H_2O using nonstoichiometric ceria, Science 330 (2010) 1797–1801, http://dx.doi.org/10.1126/science.1197834.

[23] S. Abanades, G. Flamant, Thermochemical hydrogen production from a two-step solar-driven water-splitting cycle based on cerium oxides, Sol. Energy 80 (2006) 1611–1623, http://dx.doi.org/10.1016/j.solener.2005.12.005.

[24] W.C. Chueh, S.M.W.C. Haile, A thermochemical study of ceria: exploiting an old material for new modes of energy conversion and CO_2 mitigation, Phil. Trans. R. Soc. A 368 (2010) 3269–3294, http://dx.doi.org/10.1098/rsta.2010.0114.

[25] M. Mogensen, N.M. Sammes, G.A. Tompsett, Physical, chemical and electrochemical properties of pure and doped ceria, Solid State Ionics 129 (2000) 63–94, http://dx.doi.org/10.1016/S0167-2738(99)00318-5.

[26] D.R. Mullins, The surface chemistry of cerium oxide, Surf. Sci. Rep. 70 (2015) 42–85, http://dx.doi.org/10.1016/j.surfrep.2014.12.001.

[27] S. Abanades, A. Le Gal, A. Cordier, G. Peraudeau, G. Flamant, A. Julbe, Investigation of reactive cerium-based oxides for H_2 production by thermochemical two-step water-splitting, J. Mater. Sci. 45 (2010) 4163–4173, http://dx.doi.org/10.1007/s10853-010-4506-4.

[28] A. Le Gal, S. Abanades, Catalytic investigation of ceria-zirconia solid solutions for solar hydrogen production, Int. J. Hydrog. Energy 36 (2011) 4739–4748, http://dx.doi.org/10.1016/j.ijhydene.2011.01.078.

[29] F. Call, M. Roeb, M. Schmücker, C. Sattler, R. Pitz-Paal, Ceria doped with zirconium and lanthanide oxides to enhance solar thermochemical production of fuels, J. Phys. Chem. C 119 (2015) 6929–6938, http://dx.doi.org/10.1021/jp508959y.

[30] A. Bonk, A.C. Maier, M.V.F. Schlupp, D. Burnat, A. Remhof, R. Delmelle, A. Steinfeld, U.F. Vogt, The effect of dopants on the redox performance, microstructure and phase formation of ceria, J. Power Sources 300 (2015) 261–271, http://dx.doi.org/10.1007/978-981-287-724-6_2.

[31] S. Lorentzou, G. Karagiannakis, D. Dimitrakis, C. Pagkoura, A. Zygogianni, A.G. Konstandopoulos, Thermochemical redox cycles over Ce-based oxides, Energy Procedia 69 (2015) 1800–1809, http://dx.doi.org/10.1016/j.egypro.2015.03.152.

[32] S. Haussener, A. Steinfeld, Effective heat and mass transport properties of anisotropic porous ceria for solar thermochemical fuel generation, Materials 5 (2012) 192–209, http://dx.doi.org/10.3390/ma5010192.

[33] R.B. Chandran, J.H. Davidson, Model of transport and chemical kinetics in a solar thermochemical reactor to split carbon dioxide, Chem. Eng. Sci. 146 (2016) 302–315, http://dx.doi.org/10.1016/j.ces.2016.03.001.

[34] L.J. Venstrom, N. Petkovich, S. Rudisill, A. Stein, J.H. Davidson, The oxidation of macroporous cerium and cerium-zirconium oxide for the solar thermochemical production of fuels, Proceedings of ASME 2011 5th International Conference on Energy Sustainability; 2011, August 7–10, Washington DC, USA, Paper No. ES2011-54160, 2011, pp. 1585–1593, , http://dx.doi.org/10.1115/ES2011-54160.

[35] S.G. Rudisill, L.J. Venstrom, N.D. Petkovich, T. Quan, N. Hein, D.B. Boman, J.H. Davidson, A. Stein, Enhanced oxidation kinetics in thermochemical cycling of CeO_2 through templated porosity, J. Phys. Chem. C 117 (2013) 1692–1700, http://dx.doi.org/10.1021/jp309247c.

[36] P. Furler, J. Scheffe, D. Marxer, M. Gorbar, A. Bonk, U. Vogt, A. Steinfeld, Thermochemical CO_2 splitting via redox cycling of ceria reticulated foam structures with dual-scale porosities, Phys. Chem. Chem. Phys. 16 (2014) 10503–10511, http://dx.doi.org/10.1039/c4cp01172d.

[37] S. Ackermann, M. Takacs, J. Scheffe, A. Steinfeld, Reticulated porous ceria undergoing thermochemical reduction with high-flux irradiation, Int. J. Heat Mass Transfer 107 (2017) 439–449, http://dx.doi.org/10.1016/j.ijheatmasstransfer.2016.11.032.

[38] P. Furler, J. Scheffe, M. Gorbar, L. Moes, U. Vogt, A. Steinfeld, Solar thermochemical CO_2 splitting utilizing a reticulated porous ceria redox system, Energy Fuels 26 (2012) 7051–7059, http://dx.doi.org/10.1021/ef3013757.

[39] M. Singh, J. Martínez-Fernández, A.R. Arellano-López, Environmentally conscious ceramics (ecoceramics) from natural wood precursors, Curr. Opin. Solid State Mater. Sci. 7 (2003) 247–254, http://dx.doi.org/10.1016/j.cossms.2003.09.004.

[40] C.D. Malonzo, R.M. De Smith, S.G. Rudisill, N.D. Petkovich, J.H. Davidson, A. Stein, Wood-templated CeO_2 as active material for thermochemical CO production, J. Phys. Chem. C 118 (2014) 26172–26181, http://dx.doi.org/10.1021/jp5083449.

[41] R.C. Pullar, P. Marques, J. Amaral, J.A. Labrincha, Magnetic wood-based biomorphic $Sr_3Co_2Fe_{24}O_{41}$ Z-type hexaferrite ecoceramics made from cork templates, Mater. Design 82 (2015) 297–303, http://dx.doi.org/10.1016/j.matdes.2015.03.047.

[42] R.C. Pullar, L. Gil, F.A.C. Oliveira, Biomimetic cork-based CeO_2 ecoceramics for hydrogen generation using concentrated solar energy, Ciência & Tecnologia dos Materiais 28 (2016) 23–28, http://dx.doi.org/10.1016/j.ctmat.2016.04.002.

[43] R.C. Pullar, R.M. Novais, Cork-based biomimetic ceramic 3-DOM foams, Mater.

Today 20 (2017) 45–46, http://dx.doi.org/10.1016/j.mattod.2016.12.004.
[44] L. Gil, Cork: a strategic material, Front. Chem. 2 (2014) 1–2, http://dx.doi.org/10.3389/fchem.2014.00016 Article 16.
[45] H. Pereira, Cork: Biology, Production and Uses, 1st ed., Elsevier Science B.V., Amsterdam, 2007.
[46] APCOR, Yearbook 2016, Portuguese Cork Association (Portugal). https://www.apcor.pt/ (accessed 10 May 2018).
[47] F.A.C. Oliveira, S. Dias, J. Mascarenhas, J.M.F. Ferreira, S. Olhero, D. Dias, Fabrication of cellular cordierite foams, in: R. Martins, E. Fortunato, I. Ferreira, C. Dias (Eds.), Adv. Mater. Forum II, 455-456, Trans Tech Publications, Switzerland, 2004, pp. 177–181, , http://dx.doi.org/10.4028/www.scientific.net/MSF.455-456.177.
[48] M.J. Matos, M.F. Vaz, J.C. Fernandes, F.A.C. Oliveira, Structure of cellular cordierite foams, in: R. Martins, E. Fortunato, I. Ferreira, C. Dias (Eds.), Adv. Mater. Forum II, 455-456, Trans Tech Publications, Switzerland, 2004, pp. 163–167, , http://dx.doi.org/10.4028/www.scientific.net/MSF.455-456.163.
[49] A. Le Gal, S. Abanades, G. Flamant, CO_2 and H_2O splitting for thermochemical production of solar fuels using nonstoichiometric ceria and ceria/zirconia solid solutions, Energy Fuels 25 (2011) 4836–4845, http://dx.doi.org/10.1021/ef200972r.
[50] G. Levêque, S. Abanades, Design and operation of a solar-driven thermogravimeter for high temperature kinetic analysis of solid–gas thermochemical reactions in controlled atmosphere, Sol. Energy 105 (2014) 225–235, http://dx.doi.org/10.1016/j.solener.2014.03.022.
[51] M.M. Nair, S. Abanades, Tailoring hybrid nonstoichiometric ceria redox cycle for combined solar methane reforming and thermochemical conversion of H_2O/CO_2, Energy Fuels 30 (2016) 6050–6058, http://dx.doi.org/10.1021/acs.energyfuels.6b01063.
[52] P. Fornasiero, G. Balducci, R. Di Monte, J. Kašpar, V. Sergo, G. Gubitosa, A. Ferrero, M. Graziani, Modification of the redox behaviour of CeO_2 induced by structural doping with ZrO_2, J. Catal. 164 (1996) 173–183, http://dx.doi.org/10.1006/jcat.1996.0373.
[53] N.R. Rhodes, M.M. Bobek, K.M. Allen, D.W. Hahn, Investigation of long term reactive stability of ceria for use in solar thermochemical cycles, Energy 89 (2015) 924–931, http://dx.doi.org/10.1016/j.energy.2015.06.041.
[54] R.D. Shannon, Revised effective ionic radii and systematic studies of interatomic distances in halides and chalcogenides, Acta Cryst. A 32 (1976) 751–767, http://dx.doi.org/10.1107/S0567739476001551.
[55] F. Call, M. Roeb, M. Schmücker, H. Bru, D. Curulla-Ferre, C. Sattler, R. Pitz-Paal, Thermogravimetric analysis of zirconia-doped ceria for thermochemical production of solar fuel, Am. J. Analyt. Chem. 4 (2013) 37–45, http://dx.doi.org/10.4236/ajac.2013.410A1005.
[56] M. Takacs, S. Ackermann, A. Bonk, M. Neises-von Puttkamer, P. Haueter, J.R. Scheffe, U.F. Vogt, A. Steinfeld, Splitting CO_2 with a ceria-based redox cycle in a solar-driven thermogravimetric analyzer, AIChE J. 63 (2017) 1263–1271, http://dx.doi.org/10.1002/aic.15501.
[57] F.A.C. Oliveira, High temperature corrosion of ceramic foam radiant gas burners, The European corrosion congress, Proceedings EUROCORR 2005, Lisbon - Portugal, 4–8 September, 2005, EFC Event No. 273 (CD Proceedings) Paper 125, 2005, pp. 1–10.
[58] A.C. Tas, M. Akinc, Phase relations in the system Al_2O_3-$Ce_2Si_2O_7$ in the temperature range 900° to 1925 °C in inert atmosphere, J. Am. Ceram. Soc. 76 (1993) 1595–1601, http://dx.doi.org/10.1111/j.1151-2916.1993.tb03945.x.
[59] A.C. Tas, M. Akinc, Phase relations in the system Ce_2O_3–$Ce_2Si_2O_7$ in the temperature range 1150° to 1970 °C in reducing and inert atmospheres, J. Am. Ceram. Soc. 77 (1994) 2953–2960, http://dx.doi.org/10.1111/j.1151-2916.1994.tb04530.x.
[60] A.S. Ivanova, Physicochemical and catalytic properties of systems based on CeO_2, Kinet. Catal. 50 (2009) 797–815, http://dx.doi.org/10.1134/S0023158409060020.
[61] D. Terribile, A. Trovarelli, J. Llorca, C. Leitenburg, G. Dolcetti, The synthesis and characterization of mesoporous high-surface area ceria prepared using a hybrid organic/inorganic route, J. Catal. 178 (1998) 299–308, http://dx.doi.org/10.1006/jcat.1998.2152.
[62] C. Bueno-Ferrer, S. Parres-Esclapez, D. Lozano-Castelló, A. Bueno-López, Relationship between surface area and crystal size of pure and doped cerium oxides, J. Rare Earths 28 (2010) 647–653, http://dx.doi.org/10.1016/S1002-0721(09)60172-1.
[63] A. Le Gal, S. Abanades, Dopant incorporation in ceria for enhanced water-splitting activity during solar thermochemical hydrogen generation, J. Phys. Chem. C 116 (2012) 13516–13523, http://dx.doi.org/10.1021/jp302146c.
[64] B. Bulfin, A.J. Lowe, K.A. Keogh, B.E. Murphy, O. Lübben, S.A. Krasnikov, I.V. Shvets, Analytical model of CeO_2 oxidation and reduction, J. Phys. Chem. C 117 (2013) 24129–24137, http://dx.doi.org/10.1021/jp406578z.
[65] V.M. Wheeler, R. Bader, P.B. Kreider, M. Hangi, S. Haussener, W. Lipiński, Modelling of solar thermochemical reaction systems, Sol. Energy 156 (2017) 149–168, http://dx.doi.org/10.1016/j.solener.2017.07.069.
[66] I. Ermanoski, Maximizing efficiency in two-step solar-thermochemical fuel production, Energy Procedia 69 (2015) 1731–1740, http://dx.doi.org/10.1016/j.egypro.2015.03.141.